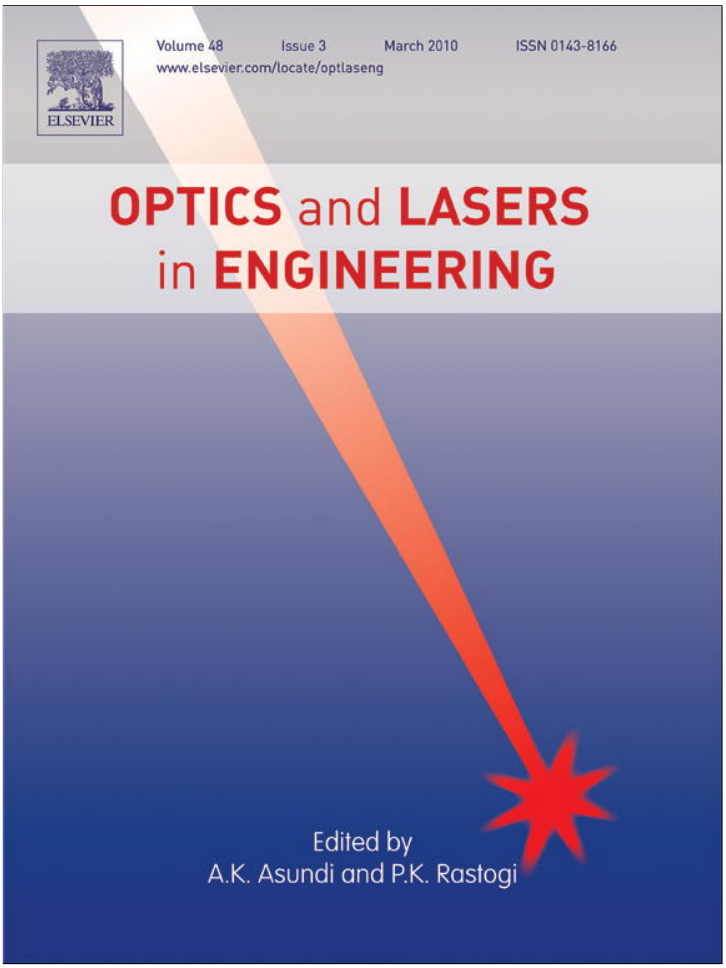

Optics and Lasers in Engineering 48 (2010) 257–267

Contents lists available at ScienceDirect

Optics and Lasers in Engineering

journal homepage: www.elsevier.com/locate/optlaseng

Review

Surface carburizing of Ti–6Al–4V alloy by laser melting

A.F. Saleh [a], J.H. Abboud [b], K.Y. Benyounis [c,*]

[a] Department of Mechanical Engineering, University of Omer Almukhtar, P. O. Box 390M Elbyada, Libya
[b] Department of Mechanical Engineering, Garyounis University, P. O. Box 1308, Benghazi, Libya
[c] Department of Industrial Engineering, Garyounis University, P. O. Box 1308, Benghazi, Libya

ARTICLE INFO

Article history:
Received 18 June 2008
Received in revised form
30 October 2009
Accepted 3 November 2009
Available online 4 December 2009

Keywords:
Titanium
Laser melting
Carburizing
Microstructure
Solidification

ABSTRACT

Surface carburizing of a Ti–6Al–4V alloy using laser melting has been investigated experimentally, with the aim of increasing surface hardness and hence improving related properties such as wear and erosion resistance. The surface of the material was coated with graphite prior to laser irradiation. Carburizing was achieved by a laser alloying mechanism, which includes melting the substrate and dissolution of the graphite in the liquid state. Two different types of lasers were used: (i) a continuous wave CO_2 (CW CO_2) laser with a maximum power of 3 kW, and (ii) a pulsating Nd–YAG laser with a maximum power per pulse of 100 W. Optical microscopy, scanning electron microscopy, EDS-analysis, and X-ray diffraction were carried out to analyze the microstructure and identify phases of the carburized layers. The results show that the carburized layers produced by CW CO_2 and Nd–YAG lasers are macroscopically homogeneous and have gradient features. The microstructures consisted of TiC crystals in the matrix of α'-Ti. The TiC crystals are either in the form of particles or dendrites. The depths to which these layers extend ranged from about 0.2–0.5 mm, depending on the treatment parameters. The volume fraction of the dendrites was found to decrease with increasing laser power or increasing traverse speed. Microhardness has been found to be directly related to the volume fraction and the size of the TiC phase. It increased to a value ranging from 500 to 800 Hv as compared to 350 Hv for the as-received substrate.

Contents

1. Introduction

The high specific strength and good corrosion resistance of titanium alloys make them suitable for many engineering applications such as jet engine compressor components, aerospace components, high pressure heat exchangers, sea water desalination plants, and petrol-chemical plants [1]. However, the wear resistance of titanium alloys is inadequate in many of these applications. Various means have been suggested for alleviating these wear problems. For example, the tribological performance of titanium alloys is much improved with nitride, carbide or oxycarbonitride coatings. Thin coatings have been prepared by many different methods such as ion radiation, chemical vapour

* Corresponding author.
E-mail addresses: elmhdi1772000@yahoo.com (A.F. Saleh), jhabboud@yahoo.com (J.H. Abboud), kybenyounis@yahoo.com (K.Y. Benyounis).

0143-8166/$ - see front matter © 2009 Elsevier Ltd. All rights reserved.
doi:10.1016/j.optlaseng.2009.11.001

deposition (CVD) and physical vapour deposition (PVD) [2–5], whereas relatively thick and localized coatings can be prepared by laser surface alloying [5–19]. A good review on surface engineering of titanium alloys can be found in Ref. [20].

Laser surface alloying (LSA) involves rapid melting, intermixing and solidification of the pre or co-deposited alloying elements with part of the underlying substrate to form an alloyed zone, confined only to the near-surface region within a very short interaction time. The process is characterized by extremely high cooling rates (10^4–10^{10} °C/s), thermal gradients (10^5–10^8 °C/m) and solidification velocities (maximum up to 30 m/s) [8]. As a consequence, laser surface alloying may extend the solid solubility limit, and result in meta-stable and novel microstructures. Majumdar and Manna [6] have improved the corrosion resistance of stainless steel by laser alloying with molybdenum. Abboud and West [7] have improved the oxidation resistance of titanium by laser alloying with aluminum and also improved the erosion resistance by injecting SiC or TiB_2 into commercially pure Ti and Ti alloys [8,9]. LSA with nitrogen was also the subject of many investigators [10–14] and hardness values of more than 1000 Hv were achieved. Cracking was identified as a major problem in laser nitriding although crack free layers were obtained in some investigations [14].

The concept of laser carburizing was initially realized through the use of graphite coatings to reduce reflectivity during laser surface hardening of steels. This served as an efficient way to increase the penetration of the radiation into the steel substrate, which had been very low for the case of a CO_2 far-infrared laser (wavelength 10.6 μm). Ever since, studies have been reported on the laser carburizing of commercial pure iron [15], plain carbon steel [16], and stainless steel [17]. The production of surface alloy layers by laser melting is influenced by a number of variables and by the interaction of these variables. The absorption of laser energy and the thermal properties of the material control the thermal history of the melt including for instance the temperature profile in the melted zone, the time during which the material remains molten, and the solidification rates [15].

In the present study, the surface melting by laser irradiation was investigated as a process capable of producing a binary titanium–carbon coating, made of metallic titanium reinforced with TiC ceramic particles. The relationships between the processing parameters and the resulting solidification microstructures and microhardness profile across the carburized layers were studied experimentally.

2. Materials and experimental methods

2.1. Material and sample preparation

Commercial Ti–6Al–4V was used as a base alloy in the present study. Samples of size $100 \times 100 \times 10$ mm^3 were cut into pieces, each one 20×20 mm^2. Before laser melting, the surface of the specimen was abraded with 500 grit SiC papers, and then cleaned with methanol. Graphite powder with an average particle size of 1 μm, blended with diluted polyvinyl alcohol solution was coated on to the sample surface to a thickness of approximately 200 μm. After the layer was dried, the surface was ground with 800 grid emery paper to remove excessive material and make the surface flat and uniform.

2.2. Laser melting

Surface melting using a 3 kW CO_2 continuous wave laser (λ=10.6 μm) and a pulsed Nd–YAG laser (λ=1.06 μm) with a maximum power of 100 W, was carried out at the Technical Research Center, Tripoli, Libya. The distance between the focus beam and the specimen surface was kept at 10 mm; this distance gave a laser beam diameter of nearly 2 mm. To ensure a stable laser struck the substrate, the titanium substrate was fixed on an *X–Y* table by two metallic pieces situated on both sides. During laser melting, the laser beam struck the metallic piece before it reached the Ti sample. The schematic diagram of the setup is shown in Fig.1. Fig. 2 shows a photograph of the actual setup used during experimentation. The same setting was used for surface

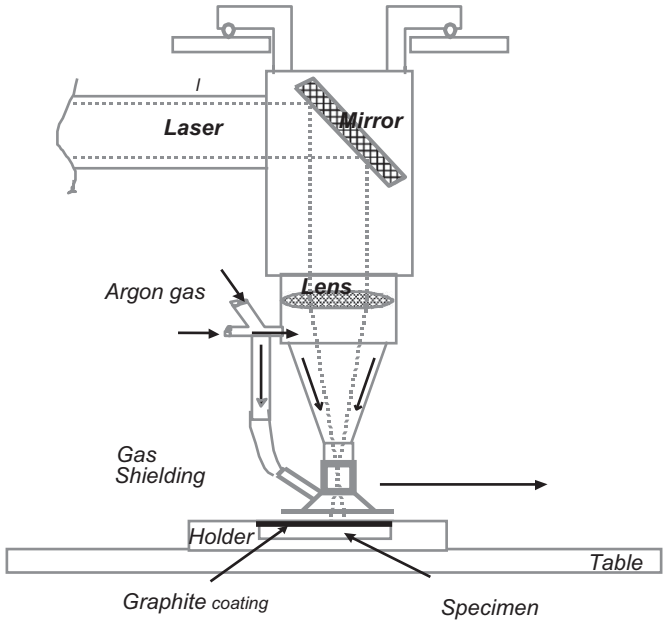

Fig. 1. A schematic diagram of the laser carburizing experimental setup.

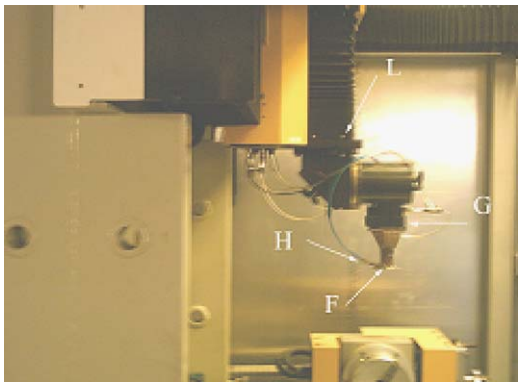

Fig. 2. Photographs showing the actual setup used: (F) Shrouding device, (H) side nozzle, (G) laser head and (L) mirror.

Table 1
Operating parameters ranges.

Parameters	Variable ranges
Type of laser	CW CO_2, Nd–YAG
Laser power	(i) CW CO_2, 1000–3000 W. (ii) Pulsating Nd–YAG, 40–60 W per pulse
Scanning speed	(i) CW CO_2, 600–1800 mm/min. (ii) Pulsating Nd–YAG, 30 and 60 mm/min

Table 2
Laser processing parameters used and the corresponding depth and microhardness of the carburized layers.

Specimen No.	Type of laser	Laser power, W	Scanning speed, mm/min	Carburized depth, mm	Microhardness at depth 0.2 mm below the surface+20 Hv
1–1	CW CO_2	1000	1000	0.2	640
1–2	CW CO_2	1500	1000	0.24	650
1–3	CW CO_2	2000	1000	0.28	600
1–4	CW CO_2	2500	1000	0.35	560
1–5	CW CO_2	3000	1000	0.4	525
2–1	CW CO_2	2000	600	0.4	700
2–2	CW CO_2	2000	900	0.33	800
2–3	CW CO_2	2000	1200	0.3	615
2–4	CW CO_2	2000	1500	0.23	480
2–5	CW CO_2	2000	1800	0.18	550
3–1	Nd–YAG, pulse	40 per pulse	30	0.28	650
3–2	Nd–YAG, pulse	50 per pulse	30	0.33	650
3–3	Nd–YAG, pulse	60 per pulse	30	0.5	700
4–1	Nd–YAG, pulse	40 per pulse	60	0.26	670
4–2	Nd–YAG, pulse	50 per pulse	60	0.32	700
4–3	Nd–YAG, pulse	60 per pulse	60	0.44	700

nitriding of titanium except the nitrogen gas was replaced by argon gas [23]. The operating parameters listed in Table 1 were selected based on the earlier studies [23] and setup constraints. Details of the experimental plan and approach are given in Table 2. The parameters under consideration were namely the type of laser, the laser power (W), and the scanning speed (mm/min). The corresponding outputs, carburized depth and microhardness are shown in the test results (Table 2). The carburized depth, is the distance from the top surface to the lower part where the TiC particles could be found and it is equal to the penetration depth when a CO_2 laser was used. It was measured by a the micrometer attached to the microhardness tester while microhardness values were being measured at a depth 0.2 mm below the surface using a 100 g load.

2.3. Surface characterization method

After the laser surface melting, the specimens were cut transversely to the direction of the laser track. The track cross-sections were prepared, ground and polished by standard metallographic techniques. The polished samples were etched chemically in a solution of $HF+HNO_3$ in alcohol. After etching, the specimens were cleaned by water and methanol, and then dried by blasting with hot air. Optical microscopy and scanning electron microscopy (SEM, model LEO 1430 VP) were used for detailed metallographic studies. For X-ray diffraction (XRD) analysis of the specimen, it was necessary to melt a wide area by overlapping the laser tracks by 50%. The width of the overlapped layer was 1 cm. XRD patterns were taken using a conventional diffractometer utilizing Cukα radiation and operating at 40 kV and 20 mA. A 2θ scan range from 30° to 100°, at a speed of 0.1°/20 s, was employed. The X-ray diffraction pattern provided data normally for top surface after slight grinding and polishing. A microhardness profile across the depth was carried out with a Reichter microhardness tester using a 100 g load on metallographically polished and lightly etched track cross-sections.

3. Experimental results and discussion

3.1. Morphology and microhardness

Fig. 3 shows section profiles of the carburized layer produced at different laser powers. The top surface became rougher and the penetration depth became deeper as the power increased. The maximum carburized depth increased from 0.2 mm at 1 kW to 0.4 mm at 3 kW. The interface between the alloyed zone (AZ) and the substrate was planar and changed from flat type at low power to wavy and irregular at 2 kW. Furthermore, the planar geometry of the AZ–substrate interface penetrated considerably inside the substrate when high power was used. The irregular shape of the interface (Fig. 3b) was perhaps due to the change of laser beam shape with increasing laser power. The use of high laser power, though it increased the depth and allowed better scope of dissolution and intermixing of graphite, may at the same time have deteriorated the surface contour and led to the formation of a crater (Fig. 3c); a vigorous convective mass flow within the alloyed zone indicated by differential contours (dark and bright) in the alloyed zone is seen in Figs. 3b–d. Furthermore, the difference in etching contrast suggests that the composition in the alloyed zone was not uniform. Anthony and Cline [24] attributed the development of such a non-uniform contour or rippling to the temperature gradient, which causes high surface tension gradients between the molten liquid at the surface and bottom of the alloyed zone.

Fig. 4 presents the microhardness profile across these tracks as a function of the distance from the top of the Ti–6Al–4V alloy specimen. It shows that microhardness in the alloyed zone varied from 500 to 1050 Hv which is about 3 times harder than the hardness of 200 Hv in the substrate region. Generally, the hardness profile across the carburized layers was not uniform and has different levels of steepness depending on the track processing power. This was because of carbon concentration variation in the surface region which cased a different microstructure to develop in this region. Using 3 kW laser power, a hardness value of 650 Hv extended from the surface to a depth of 0.5 mm, while the hardness of the track produced using low power (1 kW) had a value of 1050 Hv near the surface but decreased rapidly over a short distance of about 0.1–0.15 mm from the surface. At a distance of 0.2 mm from the surface in all cases, the hardness ranged from 500 to 650 Hv with maximum values occurring when lower laser powers (1 and 1.5 kW) were used. This might be attributed to that higher carbon/volume ratios were produced when using the 1.0 and 1.5 kW laser powers, in comparison with those produced when using the 3 kW laser power. As a consequence a high carbon concentration would have been produced in the samples processed using the lower power.

Fig. 5 presents a cross-section profile showing the macrostructure of a series of alloyed zones produced using 2 kW laser power and using different scanning speeds. It is interesting to note that alloying between the graphite and

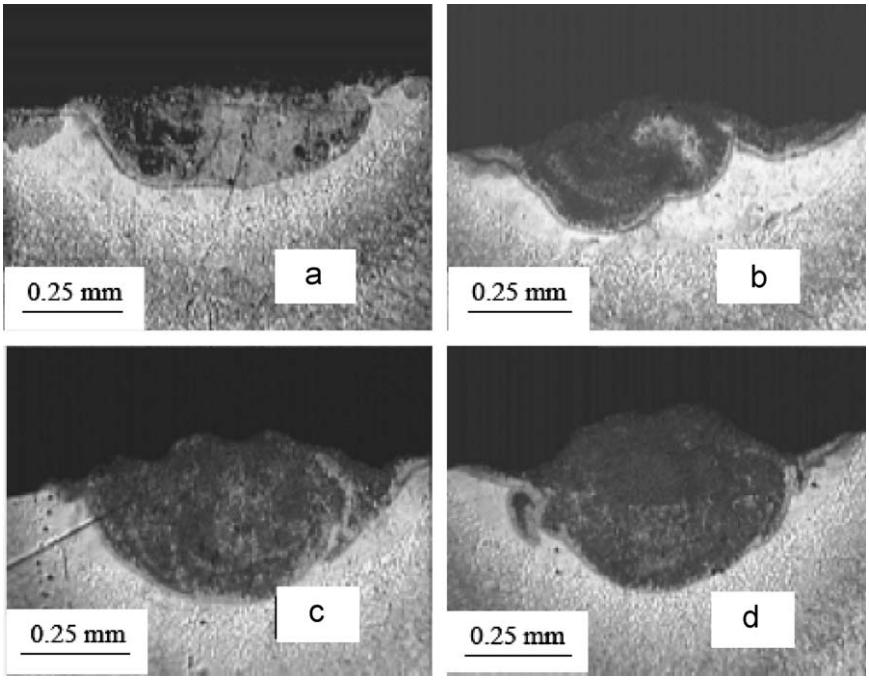

Fig. 3. Cross-sections of alloyed layers produced at constant scanning speed and different powers: (a) 1.5 kW, (b) 2.0 kW, (c) 2.5 kW, (d) 3 kW.

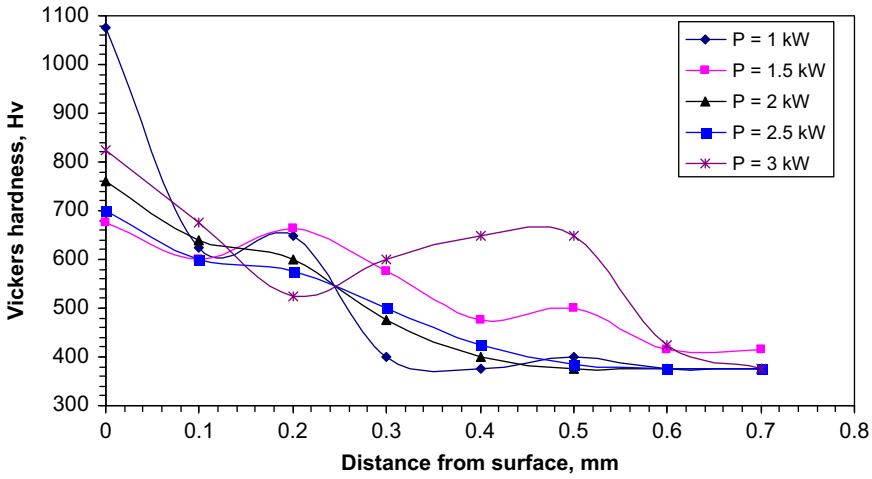

Fig. 4. Microhardness profiles across the carburized layers produced on Ti–6Al–4V at different laser powers.

the molten titanium still takes place even at fast speeds (1800 mm/min) with a penetration depth of 0.4 mm. The depth and the width of the carburized layer decreased with increasing scanning speed; however, the heat affected zones became smaller as the speed increased.

Fig. 6 shows the microhardness profiles across the carburized layers produced on the Ti–6Al–4V alloy using different scanning speeds. The general trend is that the hardness decreases with increasing laser scanning speed, the interaction time decreases as the scanning speed increases. The explanation for this seems to be that the extend of the carburizing process depends on the time of exposure to the laser, and the interaction. A uniform layer of material with a hardness distribution (700 Hv) was found when operating at a speed 600 mm/ min extended this layer to a depth of 0.3 mm below the surface. However, there is a variability in hardness values across the alloyed depth, when the scanning speed is increased as shown in Fig. 6 for speeds higher than 600 mm/min. This non-uniformity in hardness is related to the heterogeneous distribution of the dendrites within the alloyed zone.

3.2. *Microstructure and X-ray diffraction*

Previous work had shown that laser surface melting of uncoated Ti–6Al–4V alloy at 2 kW laser power and at 900 mm/min produced a layer of coarse and columnar grains extending from deep inside the specimen towards the surface; these grains contain very fine needle-like structures interpreted as Ti-martensite [16]. Microhardness measurements carried out at different locations in the melted zone showed a slight increase in hardness (380 Hv) as compared to the hardness of the substrate (350 Hv). This increase in hardness was due to a refinement of the microstructures and the formation of defects such as dislocations. No cracks were observed in the laser melted samples.

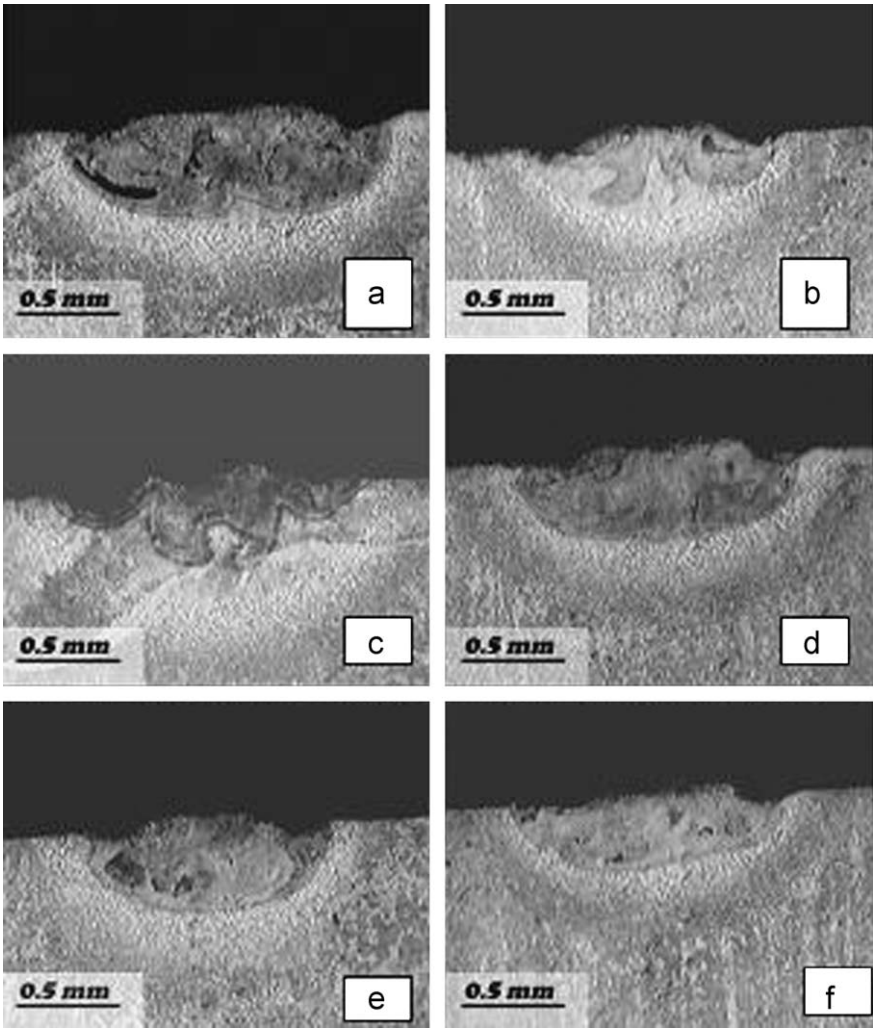

Fig. 5. Cross-sections of laser carburized layers of Ti–6Al–4V produced at 2 kW and different scanning speeds: (a) 600 mm/min, (b) 900 mm/min, (c) 1000 mm/min, (d) 1200 mm/min (e) 1500 mm/min and (f) 1800 mm/min.

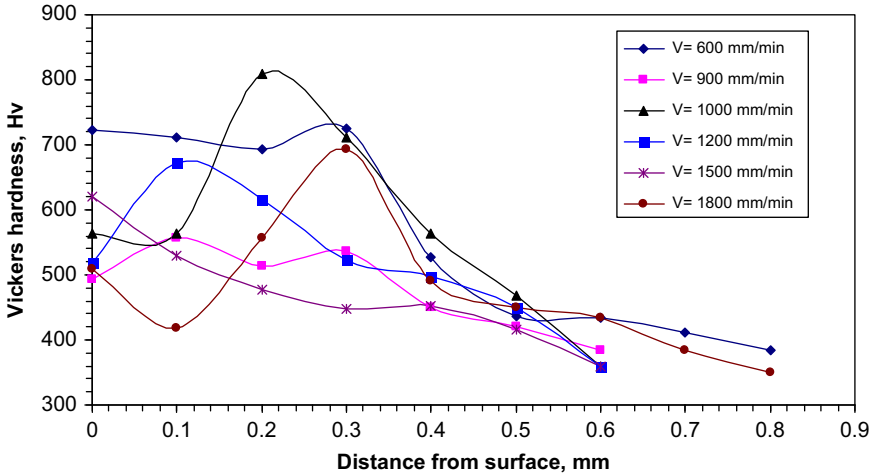

Fig. 6. Microhardness profiles across the carburized layers produced on Ti–6Al–4 V at 2 kW and different scanning speeds.

However, laser surface melting of Ti–6Al–4V alloy coated with graphite powder, also using 2 kW and 900 mm/min produced structures consisting of dendrites and network of small particles located at the grain boundaries and within the grains of a size $< 10\,\mu m$ in a matrix of needle-like structures. The distribution and the morphology of these phases are very influenced by the choice of the processing parameters (power and speed). Figs. 7a–c show the typical structure of the AZ produced at 2 kW and

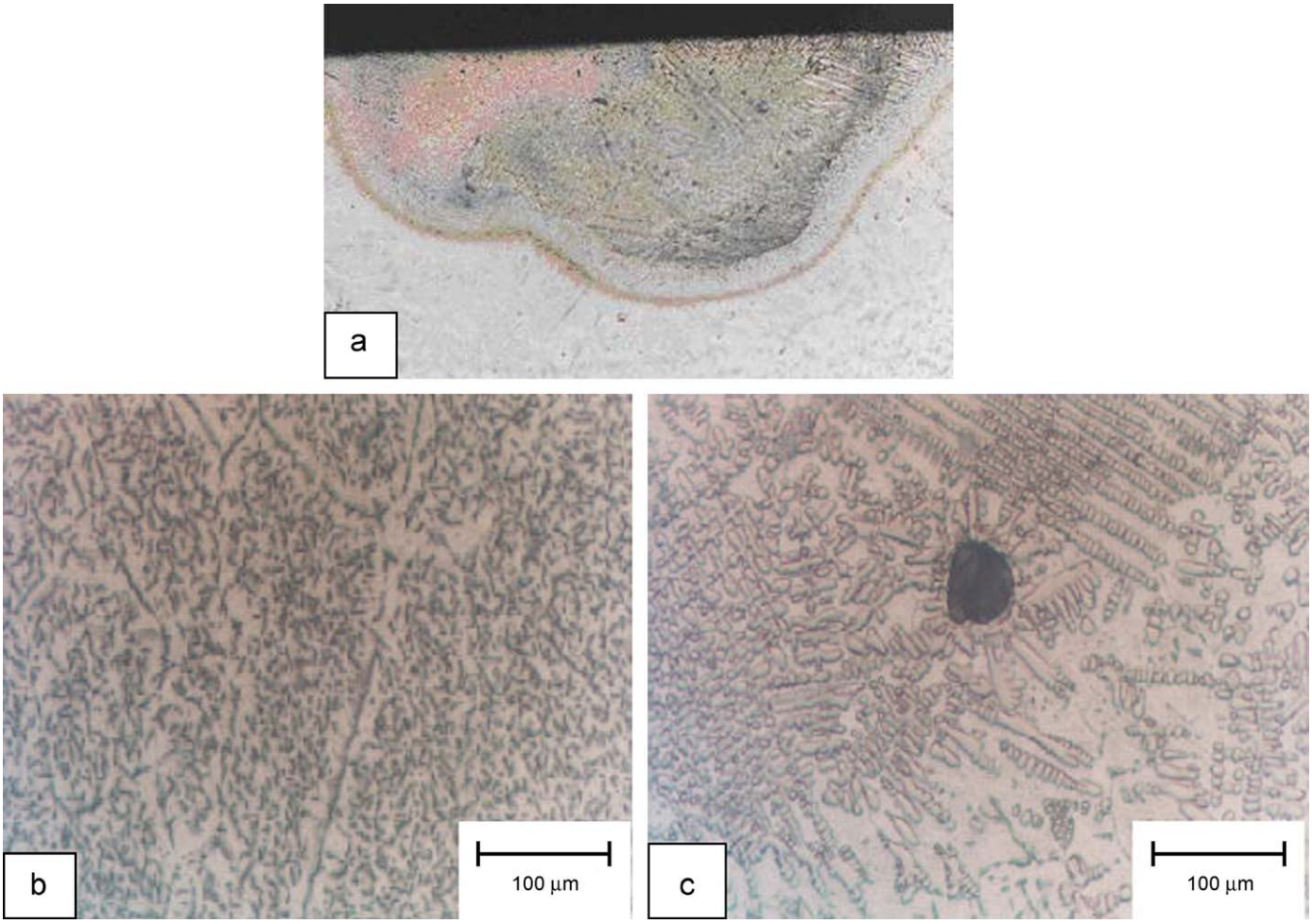

Fig. 7. Optical micrographs showing (a) cross-section of the carburized layer (2 kW and 900 mm/min) Mag. 20 ×, (b) network of particles at the grain boundaries and within the grains and (c) dendritic structure around undissolved graphite.

900 mm/min. It is evident that the present combination of power and speed has been able to achieve complete mixing between the molten titanium and the graphite power forming a Ti–C alloyed layer. No crack was visible. The alloyed zone consisted of a dendritic structure growing epitaxially from the AZ–substrate interface towards the upper surface. Few undissolved large graphite particles could be seen in the alloyed zone and where they occurred there were also dendrites which had been nucleated at the surface of the undissolved graphite particles (Fig.7c). The growth of the dendrites always followed a certain direction. The directionality of the dendrites may arise due to one dimensional heat transfer during solidification. In addition to the dendritic structure, fine particles located within the coarser grain structure and resembling a eutectic product can be seen throughout whole alloyed zone (Fig. 7b). The volume fraction of the dendrites and these particles varies with depth and depends on laser processing conditions. Scanning electron microscopy examination showed that the carburized layer has a gradient feature, i.e. the concentration of the dendrites decreased with increasing distance from the surface toward the lower part of the alloyed zone (Figs. 8a–c). The heterogeneity in the microstructure from the substrate–AZ interface towards the central and upper region of the AZ appears to suggest that the composition and effective cooling rate do no remain constant along the same direction. Fig. 8a reveals the typical microstructure of the upper region of the AZ, it consists of long primary dendritic arms growing in different directions. In the central region (Fig. 8b), the dendrites are finer with smaller secondary arm spacing.

The carburized layer produced at 1 and at 1.5 kW is very thin with dendrites growing from the surface in a direction nearly perpendicular to the surface. The layer is continuous throughout the surface. The carburized layer which had been processed at 2 kW is discontinuous and the dendrites have long arms extending into the melted region below the surface. There is also a network of smaller particles located at the grain boundaries and in the grains. The samples processed at 2.5 and at 3 kW do not have dendritic structures at all, but have a network of fine particles located between small grains ($<10\,\mu m$ in diameter) which would suggest a eutectic morphology. Below the top region, particularly at a depth of $>300\,\mu m$ from the surface, there are still no significant dendrites visible, but the network of fine particles disappears and instead there are mainly small needles visible.

In order to determine the phases present in the carburized layer, energy dispersive spectroscopy (EDS) analysis was performed on the dendrite and on some large particles at the grain boundaries and between the grains. The results of the analyses for the cases of the dendritics and large particles was a carbon content of approximately 11 wt%. This result is consistent with the analysis of TiC according to the Ti–C phase diagram and indicates that the dendrites and large particles are composed of

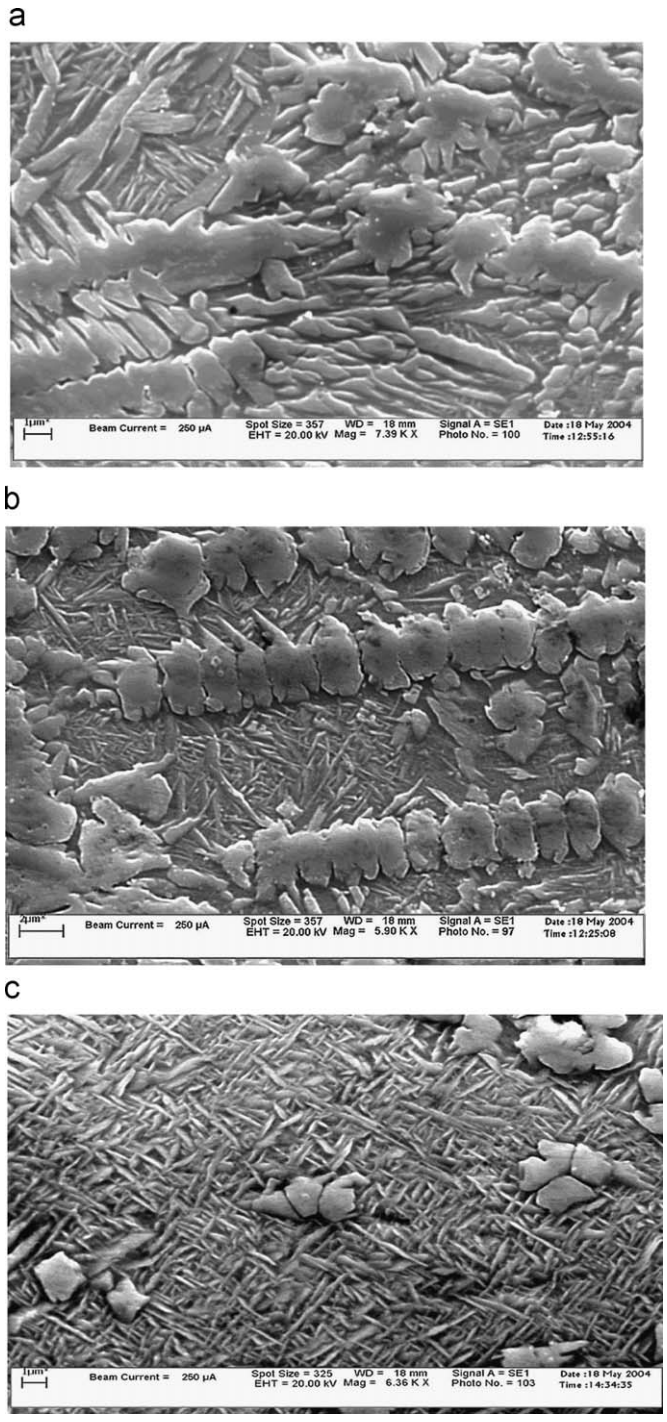

Fig. 8. SEM micrographs taking at different locations in the laser surface carburized zone (2 kW and 900 mm/min): (a) the upper zone, (b) the central zone and (c) the lower part.

TiC [22]. However, the analysis for the needle-like structures between the dendrites and these large particles indicates that only titanium, aluminum, and vanadium were present. Further analysis was carried out on sample surfaces before and after laser treatment using X-ray diffraction. The XRD analysis was performed on a selected sample (of about 1 cm^2 flat surface). The carburized layer surface width was ~1 cm produced by overlapping technique employing the same parameters used for single track. After laser melting, the surface was ground, polished and etched. The microstructures were found to be similar to those produced by single track. Figs. 9a and b show the profile of the patterns of the as-received Ti–6Al–4V alloy samples, and after laser carburizing. It is evident from the first of these patterns that the as-received alloy consists of two phases. Theses correspond to the α and β phases of pure titanium. However, the peaks of the β phase are weak. After laser carburizing, the phases seem to be mainly α′-Ti and TiC. This is consistent with the SEM micrographs which show needle-like TiC particles embedded in a needle-like structure α′ the crystal phase corresponding to α for pure sample of titanium (Fig. 8a–c).

Surface alloying of the Ti–6Al–4V alloy with carbon using the Nd–YAG laser with a focused beam produced a very smooth surface with a high depth to width ratio. The alloyed layer produced using the Nd–YAG laser extends deeper into the substrate compared with that produced by the CO_2 laser despite the lower power of the Nd–YAG laser. The maximum depth was 0.5 mm over a track of width 0.4 mm (Fig. 10). The microhardness profile across the carburized layers produced at 50 and 60 W with a speed of 30 mm/min is shown in Fig. 11. The maximum hardness values of 650 and 750 Hv can be identified with locations near the surface of the sample and lower values of hardness were measured in deeper locations. The exceptionally large increase in hardness of the AZ may be attributed to both solid solution strengthening and the presence of intermetallic TiC phase due to LSA. The value is similar to that obtained using the CW CO_2 laser, despite the lower power of the Nd–YAG laser. Apparently, the hardness development is proportional to the volume fraction and the size of the TiC phase. The gradual decrease of the hardness values in deeper layers is attributed to the gradual decrease of the TiC phase and the increase of the soft α′-Ti. The area which appears white in the macrograph has a very low hardness value, approaching the hardness of the substrate. This indicates that carbon does not penetrate to these layers perhaps due to evaporation. High turbulence loop can be seen in these graphs. Increasing the laser power led to an increase in the depth of the affected zone with a slight increase in its width also. There was also an increase in the mass flowing by convection in the alloyed zone as indicated by the different looking structure in this zone as shown in Figs. 12a and b. At high magnification, the flow pattern of the melt pool showed TiC dendrites as a denser array along the capillary flow lines. These loops were distinguished by small needle martensite microstructures at the center, and a dense array of dendrites at the periphery of the loops, i.e. along the capillary flow lines (Fig. 12b). Depending on the choice of processing parameters such as speed and power and the convection flow, different flow patterns developed and this might have caused the carbon distribution in the melt pool to become inhomogeneous, the rapid solidification further opposed extensive carbon diffusion throughout the melt. Therefore, in a single melt pool, different TiC dendrite concentrations were observed. This effect was more prominent in the tracks produced using high laser power and high speed. The carburized layers produced by the Nd–YAG laser did not show any cracks, but other types of defect such as porosity were observed. The spherical shape of the observed pores indicates that they were formed from gas bubbles, due to gas being trapped during solidification. The main sources of gases are surface contamination of the material (grease, oil, water vapour) and dissolved gas diffusion from the base material or from the organic binder used to hold the power to the surface.

An enlargement of the micrograph of the Ti–C alloyed zone produced using the Nd–YAG laser at 50 W and 30 mm/min shows a network of particles near the surface of the grains (Figs. 12b and c). The dendrites and those particles were identified by the EDS as TiC. The secondary dendrite arm spacings of the TiC are in the approximate range of 2–3 μm suggesting a very high cooling

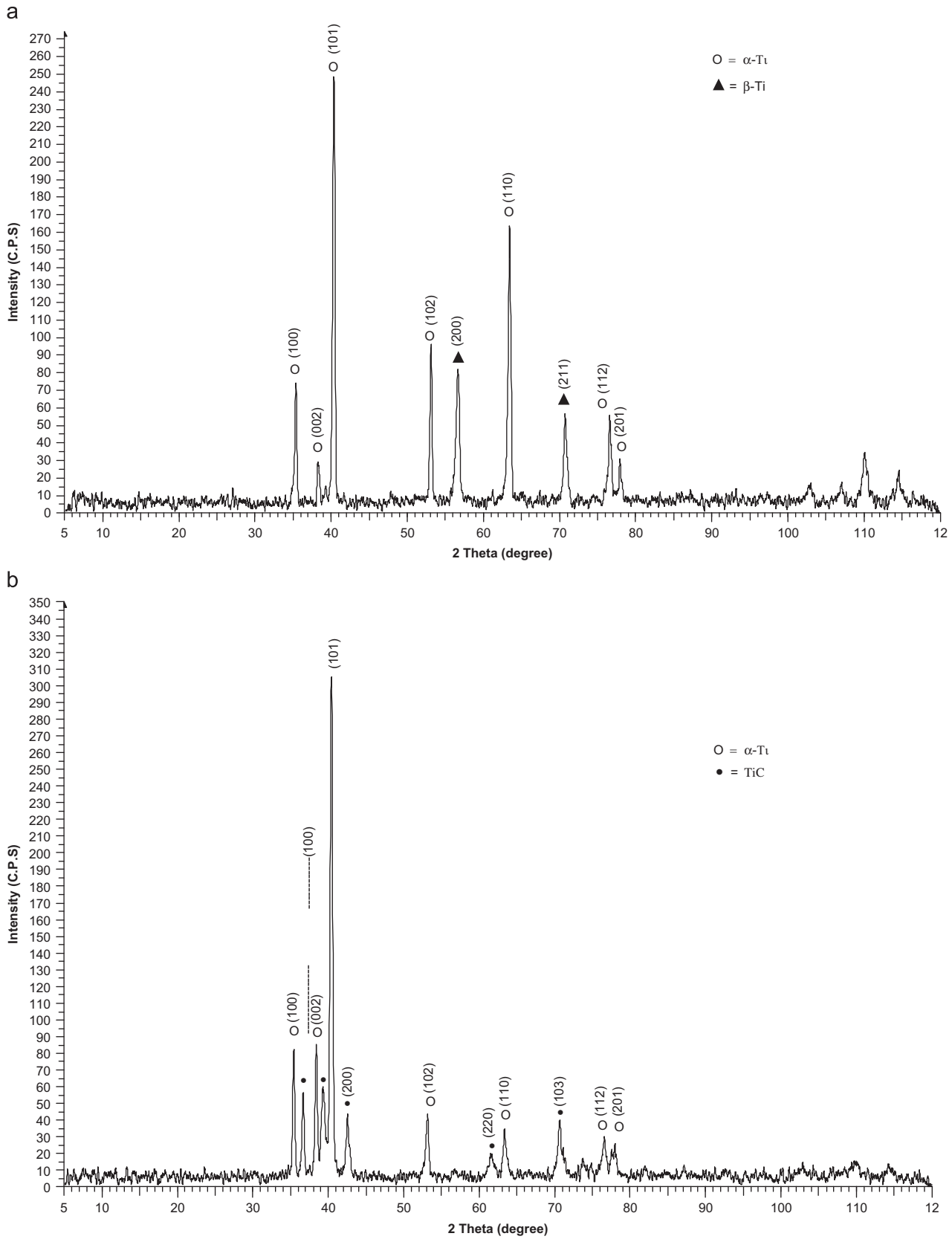

Fig. 9. X-ray diffraction patterns of the top surface of (a) Ti–6Al–4 V as received and (b) Ti–6Al–4V laser alloyed with graphite (2 kW and 900 mm/min).

rate during solidification. The average carbon content in these particles is 0.85 wt% which is slightly lower than that of the alloyed zone produced by CO_2 laser.

The microstructure after solidification of the carburized layer produced by the CO_2 laser and the ND–YAG laser can be interpreted with reference to the Ti–C phase diagram [22]. This

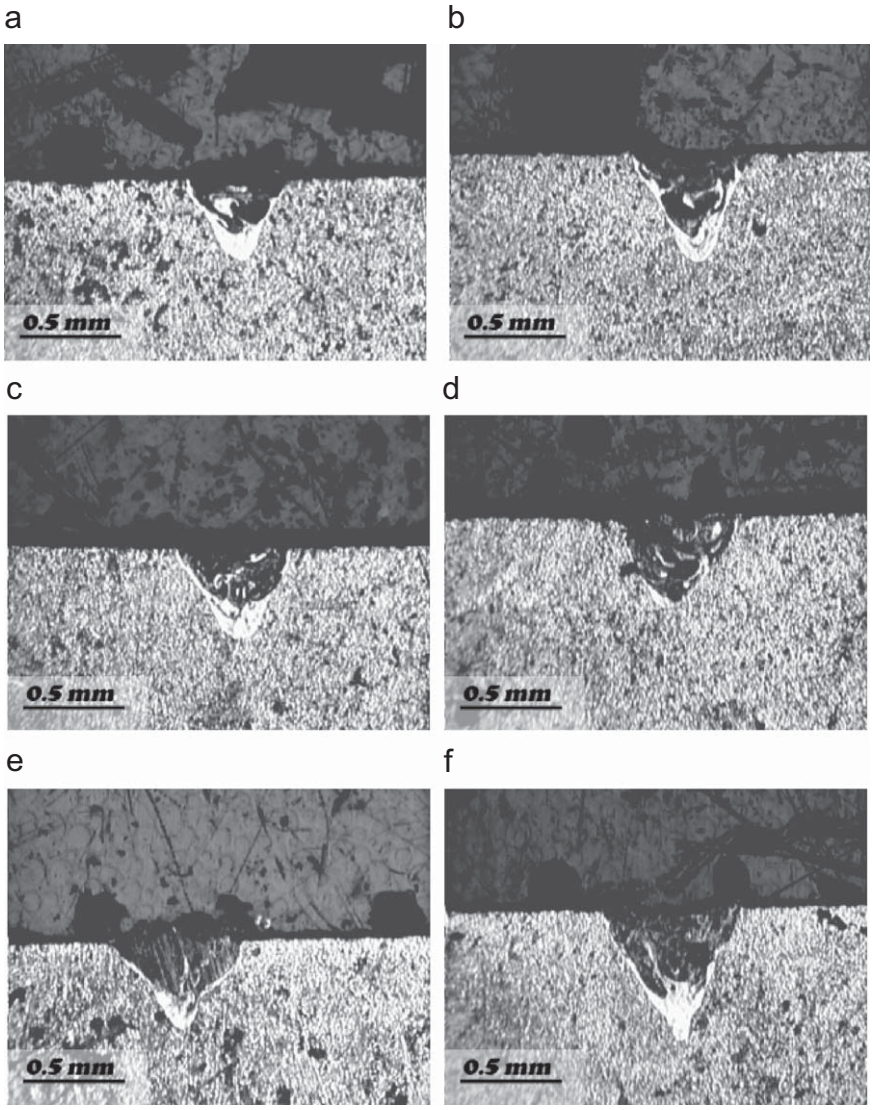

Fig. 10. Cross-sections of Ti–6Al–4V alloy surface alloyed with graphite using Nd–YAG laser at pulse width of 2.2 μs, repetition rate 10 Hz. (a) P=40 W and V=60 mm/min, (b) P=40 W and V=30 mm/min, (c) P=50 W and V=60 mm/min, (d) P=50 W and V=30 mm/min, (e) P=60 W and V=60 mm/min, (f) P=60 W and V=30 mm/min

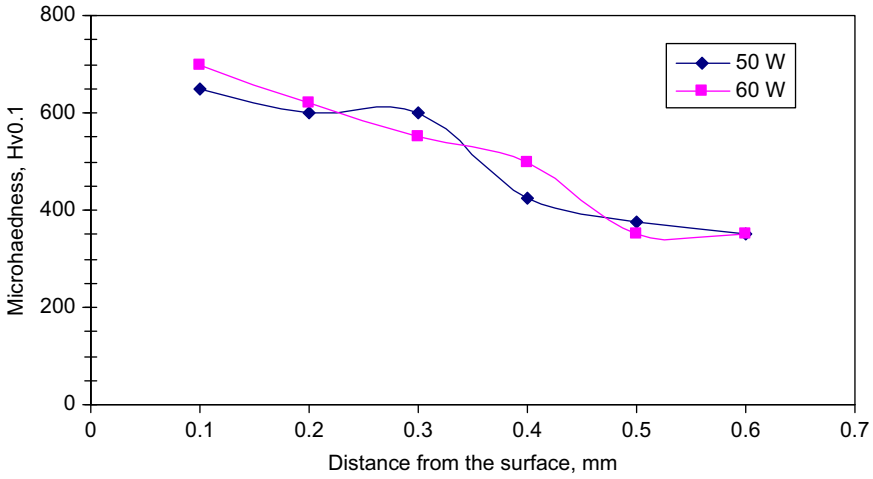

Fig. 11. Microhardness profile across the carburized layers produced by Nd–YAG laser at different powers per pulse (50 and 60 W), 30 mm/min, and 2 μs.

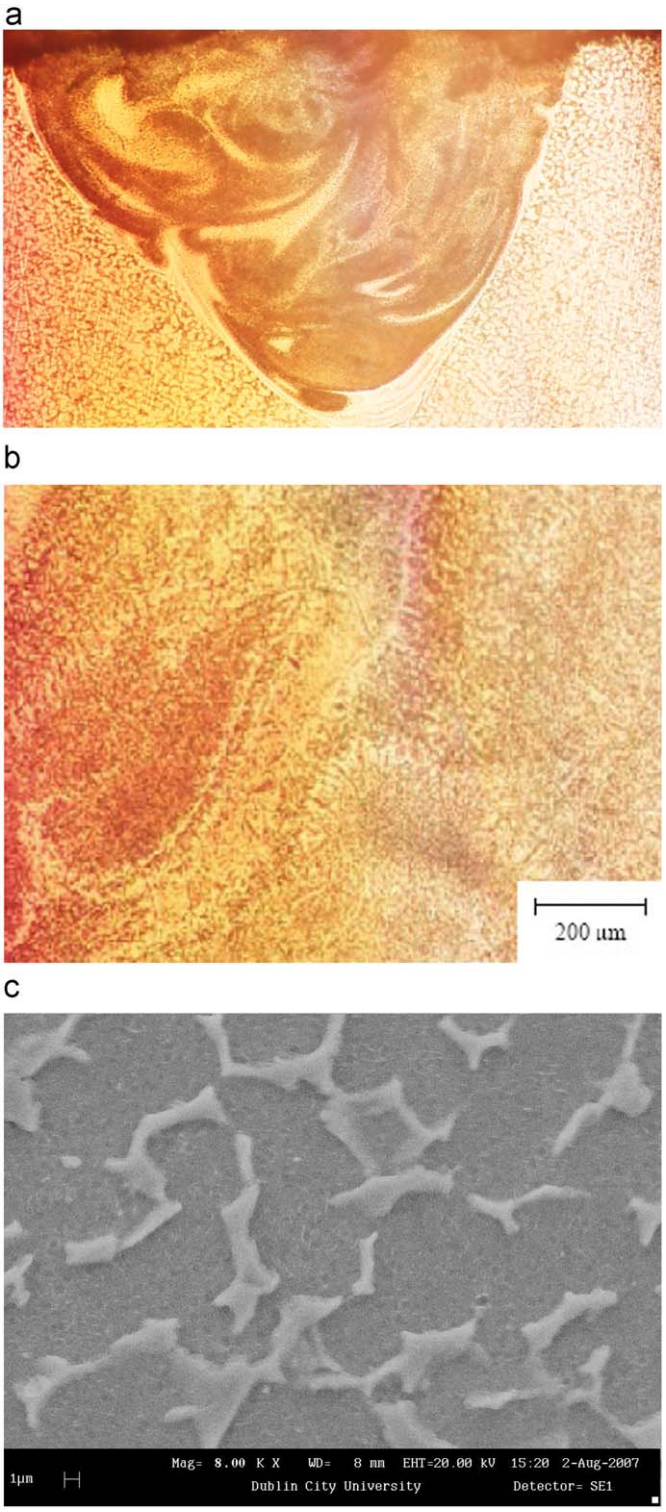

Fig. 12. (a) Optical micrograph showing titanium carburized layer produced by Nd–YAG laser operated at 50 W per pulse and speed 30 mm/min total depth is 0.33 mm, (b) optical micrograph showing dendritic structure 200 ×, and (c) SEM micrograph showing TiC at the grain boundaries.

shows TiC can exist over a wide range of stoichiometry values with a maximum melting temperature of about 3070 °C at about 16.5 wt% C. The Ti–C system forms eutectics with TiC and graphite, respectively,

$$1648\,^{\circ}\mathrm{C}\ \mathrm{Liq}(\sim 10\,\mathrm{wt\%}C) \rightarrow \beta\text{-Ti}(\sim 0.5\,\mathrm{wt\%}C) + \mathrm{TiC}(\sim 10\,\mathrm{wt\%}C)$$

$$2776\,^{\circ}\mathrm{C}\ \mathrm{Liq}(\sim 30\,\mathrm{wt\%C}) \rightarrow \mathrm{TiC}(\sim 18\,\mathrm{wt\%C} + \mathrm{graphite})$$

The carburized layers produced by laser melting of titanium coated with graphite were hypereutectic with respect to the β-Ti+TiC eutectic. Following the formation of the primary TiC dendrites, the eutectic does not form as a duplex structure, but shows only divorced morphologies; upon cooling in the solid state, β transforms to α′. The value of about 11 wt% C for the carbon content of the TiC dendrites is in reasonable agreement with the phase diagram, bearing in mind the error in the EDS procedure of determining the carbon content by difference. The hardness data of the alloyed layers (Figs. 4 and 6) show an increase as compared to the hardness of untreated titanium. These results are expected since the hardness of TiC is more than 1800 Hv [21]. The volume fraction of TiC dendrites is the dominant feature in determining overall hardness.

4. Conclusions

Laser surface melting of a titanium substrate coated with graphite powder produced a carburized layer consisting of TiC crystals in a α′-Ti matrix. The TiC appears either in the form of dendrites or as particles located inside the grains and at the grain boundaries. The microhardness of the surface region is increased significantly after carburizing and the maximum hardness achieved is 800 Hv. This extends to a depth of 0.5 mm below the surface when using low scanning speed and high power. The microhardness is a consequence of the existing volume fraction of TiC dendrites. The microstructures of the carburized layers produced by the Nd–YAG laser and the CO_2 laser are macroscopically homogeneous and have a gradient feature. The depth of the carburized layer produced by the Nd–YAG laser is greater than that produced by the CO_2 laser despite the low power of the Nd–YAG laser. Finally, LSA of Ti with carbon appears to be potential route of hardening the surface of the titanium alloys without affecting its bulk properties.

Acknowledgements

The authors wish to thank the Technical Research Center in Tajorah-Tripoli for its help in using the lasers. They also thank Dr. Osama Burshan and Prof. Bourima A. Belgasim in the Libyan Petroleum Institute (www.lpilibya.org) for the use of the SEM, and Dr Mohamed A. Al-aalam in the Industrial Research Center for the use of XRD equipment and the microhardness tester.

References

[1] Polmear J., Alloys Light, Arnold Edward, .London, 1981.
[2] Grenier M, Dube D, Adnot A, fiset M. Microstructure and wear resistance of CP titanium laser alloyed with a mixture of reactive gases. Wear 1997;210:127–135.
[3] Enomoto Y, Yamaneca K. Synthesis of titanium carbonitride films by physical vapour deposition and their structure. Thin Solid Films 1981;86:201–3.
[4] Gates AS. Composition, structure and wear resistance of TiN, TiC_xN_y and TiC coatings prepared by unbalanced magnetron sputtering techniques. Surf Coat Technol 1994;70:49–56.
[5] Randhawa H. Cathodic arc plasma deposition of TiC and TiCN films. Thin Solid Films 1987;153:209–18.
[6] Majumdar JD, Manna I. Laser surface alloying of AISI 304 stainless steel with molybdenum for improving in pitting and erosion–corrosion resistance. Mater Sci Eng 1999;267:50.
[7] Abboud JH, West DRF. Oxidation of titanium–aluminides produced by laser surface alloying. J Mater Sci Lett 1992;11:1478–82.

[8] Abboud J.H. and West D.R.F., . Titanium/ceramic composite produced by laser processing. In: Proceedings of the seventh world international conference on titanium, San Diego, California; 28 June–2 July 1992.
[9] Abboud JH, West DRF, Hibberd RH. Property assessment of laser surface treated titanium alloy. Surf Eng 1993;9:221.
[10] Sciersten M., . Surface nitriding of titanium by laser beams. In: Proceedings of the first nordic laser material processing conference, B, Thorstensen 1988. p. 66.
[11] Garcıa I, de la Fuente J, de Damborenea JJ. Ti,Al)/(Ti,Al) N coatings produced by laser surface alloying. Mater Lett 2002;53:44–51.
[12] Katayama S, Matsunawa A, Morimoto A, Ishimoto S, Arata Y. In: Surface hardening of titanium by laser nitriding. Los Angeles: ICALEO '83 LIA; 1983.
[13] Weerasighe VW, West DRF, Damborenea Jde. Laser surface nitriding of titanium and a titanium alloy. J Mater Process Technol 1996;58:79.
[14] Mridha S, Baker TN. Effects of nitrogen gas flow rates on the microstructure and properties of laser-nitrided IMI318 titanium alloy (Ti–6A1–4V). J Mater Process Technol 1998;77:115–21.
[15] Walker A, West DRF, Steen WM. Laser surface alloying of iron and 1c–1.4cr steel with carbon. Met Technol 1984;11:399–404.
[16] Abboud JH, Benyounis KY, Olabi AG, Hashmi MSJ. Laser surface treatment of iron based substrate for automotive application. J Mater Process Technol 2007;182:427–31.
[17] K.A. El-dressi, . Surface melting and alloying of some alloy steels by Nd–YAG la0ser, M.Sc. Thesis, Industrial Engineering, Garyounis University,, Fall, 2000..
[18] Ani Zhecheva Wei, Sha Savko, Malinov, Long Adrian. Enhancing the microstructure and properties of titanium alloys through nitriding and other surface engineering methods. Surf Coat Technol 2005;200:2192–207.
[19] Abboud JH, Fidel AF, Benyounis KY. Surface nitriding of Ti–6Al–4V alloy with a high power CO_2 laser. Opt Laser Technol 2008;40(2):405–14.
[20] Sha W, Malinov S. In: Titanium alloys: modelling of microstructure, properties and applications. Woodhead Publishing Limited and CRC Press; 2009.
[21] Abboud JH, West DRF. In situ production of Ti–TiC composites by laser melting. J Mater Sci Lett 1992;11:1675–7.
[22] Murray JL. In: Massalski TB, editor. Binary phase diagram, vol. 1. Ohio: American Society for Metals; 1986. p. 593.
[23] Fidel AF. Surface hardening of titanium with laser, M.Sc. thesis, Department of Mechanical Engineering, University of Garyounis, Benghazi, Libya, 2004.
[24] Anthony TR, Cline HE. Surface rippling induced by surface-tension gradients during laser surface melting and alloying. J Appl Phys 1977;48:3888.